GEOLOGY

Eccentricity-paced monsoon variability on the northeastern Tibetan Plateau in the Late Oligocene high CO_2 world

Hong Ao[1,2]*, Diederik Liebrand[3,4], Mark J. Dekkers[5], Peng Zhang[1,2], Yougui Song[1,2], Qingsong Liu[6], Tara N. Jonell[7], Qiang Sun[8], Xinzhou Li[1,2], Xinxia Li[9], Xiaoke Qiang[1], Zhisheng An[1,2]

Constraining monsoon variability and dynamics in the warm unipolar icehouse world of the Late Oligocene can provide important clues to future climate responses to global warming. Here, we present a ~4-thousand year (ka) resolution rubidium-to-strontium ratio and magnetic susceptibility records between 28.1 and 24.1 million years ago from a distal alluvial sedimentary sequence in the Lanzhou Basin (China) on the northeastern Tibetan Plateau margin. These Asian monsoon precipitation records exhibit prominent short (~110-ka) and long (405-ka) eccentricity cycles throughout the Late Oligocene, with a weak expression of obliquity (41-ka) and precession (19-ka and 23-ka) cycles. We conclude that a combination of eccentricity-modulated low-latitude summer insolation and glacial-interglacial Antarctic Ice Sheet fluctuations drove the eccentricity-paced precipitation variability on the northeastern Tibetan Plateau in the Late Oligocene high CO_2 world by governing regional temperatures, water vapor loading in the western Pacific and Indian Oceans, and the Asian monsoon intensity and displacement.

INTRODUCTION

Earth experienced sustained cooling since the Early Eocene Climate Optimum and shifted, at the Eocene-Oligocene transition [EOT; ~34 million years (Ma) before present (BP)], from a warm greenhouse state without permanent ice sheets on both poles to a cooler, but still substantially warmer than today, unipolar icehouse state with the sole continental-scale ice sheet on Antarctica (*1*). The Oligocene (23.03 to 33.9 Ma BP) is the first epoch in the newly established unipolar icehouse world. This unipolar glacial state persisted until the Pliocene-Pleistocene transition when the permanent establishment of the Greenland Ice Sheet marked the transition to a bipolar glacial state (*1*–*3*). Average global deep ocean and sea surface temperature were ~3° and >8°C higher than today during the Oligocene, respectively (*1*, *4*). Oligocene proxy records (*5*–*8*) suggest that atmospheric CO_2 concentrations were between ~400 and ~800 parts per million (ppm) before ~24.5 Ma BP, embracing the present-day and projected values for the year 2100 (*9*). At ~24.5 Ma BP, atmospheric CO_2 concentrations fell to near preindustrial levels of ~300 ppm. Present-day atmospheric CO_2 values (420 ppm) have thus exceeded simulated thresholds (~280 ppm) for Northern Hemisphere deglaciation (*10*), which raises the possibility that Earth will return to a unipolar icehouse state with a near-to-complete loss of the Greenland Ice Sheet, in addition to a collapse of the West Antarctic Ice Sheet. Thus, investigation into Oligocene climate–cryosphere interactions can provide crucial insight into such a future world and help constrain model simulations of regional responses to future global warming.

The Asian monsoon is the largest monsoon system on Earth; it governs moisture supply over a vast area, extending from the low-latitude western Pacific and Indian Oceans to mid-latitude East Asia (Fig. 1A) (*11*–*13*). The Tibetan Plateau is the world's highest topographic feature, extending over a vast region from ~70°E to ~105°E and from ~20°N to ~45°N (Fig. 1A). Since its formation, climate to the south and east of the plateau has been strongly affected by the Asian monsoon (*14*). The Lanzhou Basin, which is situated on the northeastern (NE) margin of the Tibetan Plateau (Fig. 1A), contains well-exposed Oligocene red mudstones that originated primarily from the surrounding mountains (*15*–*17*). The regional hydroclimate is strongly controlled by the Asian summer monsoon. A recently obtained magnetostratigraphic age model, supported by mammal and pollen biostratigraphy, demonstrates that a particular red mudstone sequence, exposed at the Duitinggou section (36°13′N, 103°37′E; 1800-m elevation) in the central Lanzhou Basin (Fig. 1, B and C), spans a (near-) continuous time interval between 28.1 and 24.1 Ma BP (*15*, *16*, *18*, *19*). Here, we use elemental and environmental magnetic records from this terrestrial sequence, which are related to regional hydroclimate fluctuations in the Lanzhou Basin (*20*, *21*), to provide insight to orbital variability and dynamics of monsoon precipitation on the NE Tibetan Plateau margin in the Late Oligocene high CO_2 world. Our results represent the first ~4-thousand year (ka) resolution Late Oligocene monsoon records from the Tibetan Plateau and thereby help fill a gap in our understanding of the orbital Asian monsoon variability and forcing dynamics in a unipolar icehouse state.

RESULTS AND DISCUSSION

High-resolution Late Oligocene NE Tibetan Plateau hydroclimate records

The Lanzhou Basin is situated in a semi-arid region of central China, where regional precipitation is predominantly delivered by the

[1]State Key Laboratory of Loess and Quaternary Geology, Institute of Earth Environment, Chinese Academy of Sciences, Xi'an, China. [2]Open Studio for Oceanic-Continental Climate and Environment Changes, Pilot National Laboratory for Marine Science and Technology (Qingdao), Qingdao, China. [3]National Oceanography Centre, European Way, SO14 3ZH Southampton, UK. [4]PalaeoClimate.Science, 27 Granby Grove, SO17 3RY, Southampton, UK. [5]Paleomagnetic Laboratory Fort Hoofddijk, Department of Earth Sciences, Faculty of Geosciences, Utrecht University, Utrecht, The Netherlands. [6]Centre for Marine Magnetism (CM2), Department of Ocean Science and Engineering, Southern University of Science and Technology, Shenzhen, China. [7]School of Geographical and Earth Sciences, University of Glasgow, Glasgow, UK. [8]College of Geology and Environment, Xi'an University of Science and Technology, Xi'an, China. [9]School of Earth Sciences, China University of Geosciences (Wuhan), Wuhan, China. *Corresponding author. Email: aohong@ieecas.cn

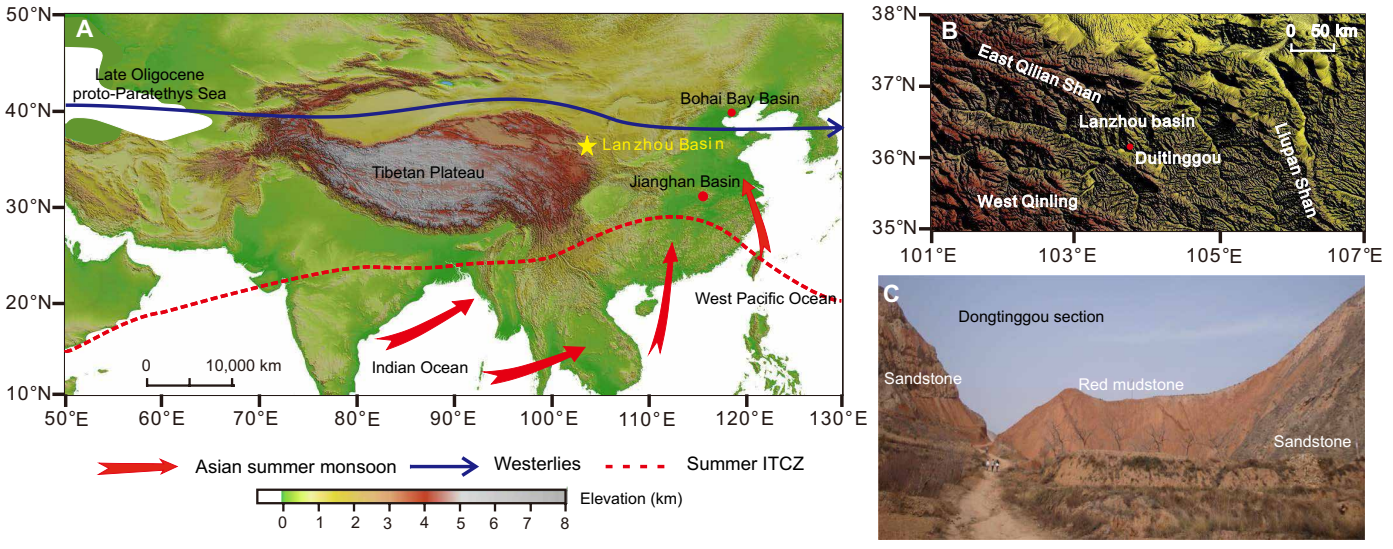

Fig. 1. Site location map and photographs. (**A**) Topographic map of Asia with schematic summer monsoon, westerlies, and summer intertropical convergence zone (ITCZ) at present (*11*) and with the Late Oligocene proto-Paratethys Sea that was located west of the Tibetan Plateau (*26*). (**B**) Topographic map of the Lanzhou Basin and surrounding mountains with the location of the studied Duitinggou section (red solid circle). (**C**) Field photograph of the tilted to the west (~30°) Duitinggou section. The left-hand side (west) is younger than the right-hand side (east). Photo credit: Hong Ao, Institute of Earth Environment, Chinese Academy of Sciences.

lower-tropospheric Asian summer monsoon moisture with a smaller additional contribution from the upper-tropospheric westerlies (Fig. 1A) (*22*). In a more regional geological context, the Lanzhou Basin is surrounded by the East Qilian Shan in the west and north, the West Qinling mountains in the south, and the Liupan Shan ridge in the east (Fig. 1B). The Late Oligocene red mudstone sequence from the Duitinggou section has a stratigraphic thickness of 105 m. It is highly expanded, contains no stratification, and has a homogeneous red color (Fig. 1C), which all indicate a stable deposition condition in a distal alluvial environment (*21*, *23*, *24*). The red color is consistent with frequent subaerial exposure leading to pedogenesis. The absence of carbonate, color mottling, and gley features indicates that the pedogenic weathering was not as intense as that in the more humid South China during the Late Oligocene. This lithological observation is consistent with a much lower regional precipitation on the northwestern margin of the summer monsoon realm. The red mudstone sequence is underlain and overlain by grayish white sandstone packages (Fig. 1C), reflective of high-gradient and more energetic fluvial deposition. The 105-m-thick red mudstone section records a continuous paleomagnetic polarity sequence from C10n.1n to C7n.2n (*15*), consistent with the Late Oligocene pollen and faunal assemblage obtained from this sequence (*16*, *18*, *19*). An age model was constructed for the period between 28.1 and 24.1 Ma BP via linear interpolation between subsequent tie points using 10 geomagnetic polarity reversals identified in the section (*15*), which were assigned the most recent astronomically calibrated ages (*1*). This paleomagnetic chronology resulted in constant sedimentation rates between reversals, which varied between 1 and 6 cm/ka throughout the study interval.

We measured hydroclimate proxies, i.e., rubidium-to-strontium ratio (Rb/Sr) and low-field magnetic susceptibility (χ_{lf}), at 10-cm stratigraphic intervals (corresponding to a ~4-ka time spacing) from the Late Oligocene red mudstones at the Duitinggou section (Fig. 2). The Rb/Sr record of Early Miocene red mudstones and sandstones in the Lanzhou Basin has been suggested to be sensitive to subtle pedogenic weathering variability (*20*), despite the prevailing low precipitation and weathering intensity. In general, higher precipitation causes stronger pedogenic weathering of the red mudstone, which depletes mobile Sr and enriches insoluble Rb, leading to higher Rb/Sr values (*20*). In addition to local magnetic mineral formation during pedogenic weathering, higher precipitation and associated stronger stream flow dynamics increases erosion and facilitates more magnetic materials to be eroded and transported from the surrounding mountains and catchment area to the deposition site. Thus, higher Rb/Sr intervals generally correlate to higher magnetic mineral concentration intervals that are marked by higher χ_{lf} values in the Late Oligocene Duitinggou mudstone sequence (Fig. 2, B and C) and are linked to periods with higher precipitation.

In contrast to the homogenous red color observed with the naked eye in the field (Fig. 1C), the 105-m-thick (4-Ma duration) Rb/Sr and χ_{lf} records from the Lanzhou Basin are characterized by distinct large-amplitude quasi-regular cycles (Fig. 2, A to C). We interpret these cycles in our hydroclimate proxy records as orbitally paced precipitation variability over the NE Tibetan Plateau during the Late Oligocene. Wavelet analyses of the Rb/Sr and χ_{lf} records on the paleomagnetic age model suggest distinct short (~110-ka) and long (405-ka) eccentricity cycles in the time series between 28.1 and 24.1 Ma BP throughout the Late Oligocene (Fig. 3, A and B). Obliquity (41-ka) and precession (19- and 23-ka) cycles are only weakly expressed (Fig. 3, A and B). Even in intervals with high sedimentation rates, such as between ~24.9 and ~26 Ma BP (254- to 290-m stratigraphic level) and between ~27.4 and ~27.9 Ma BP (314- to 332-m stratigraphic level) (Fig. 2), where higher frequencies are more prone to being preserved in principle, the eccentricity cycles are still substantially stronger compared to the obliquity and precession cycles. Orbital expression is broadly consistent between Rb/Sr and χ_{lf} records (Figs. 2 and 3), with a few relatively small differences that are possibly related to variable sensitivity of different proxy records to hydroclimate change.

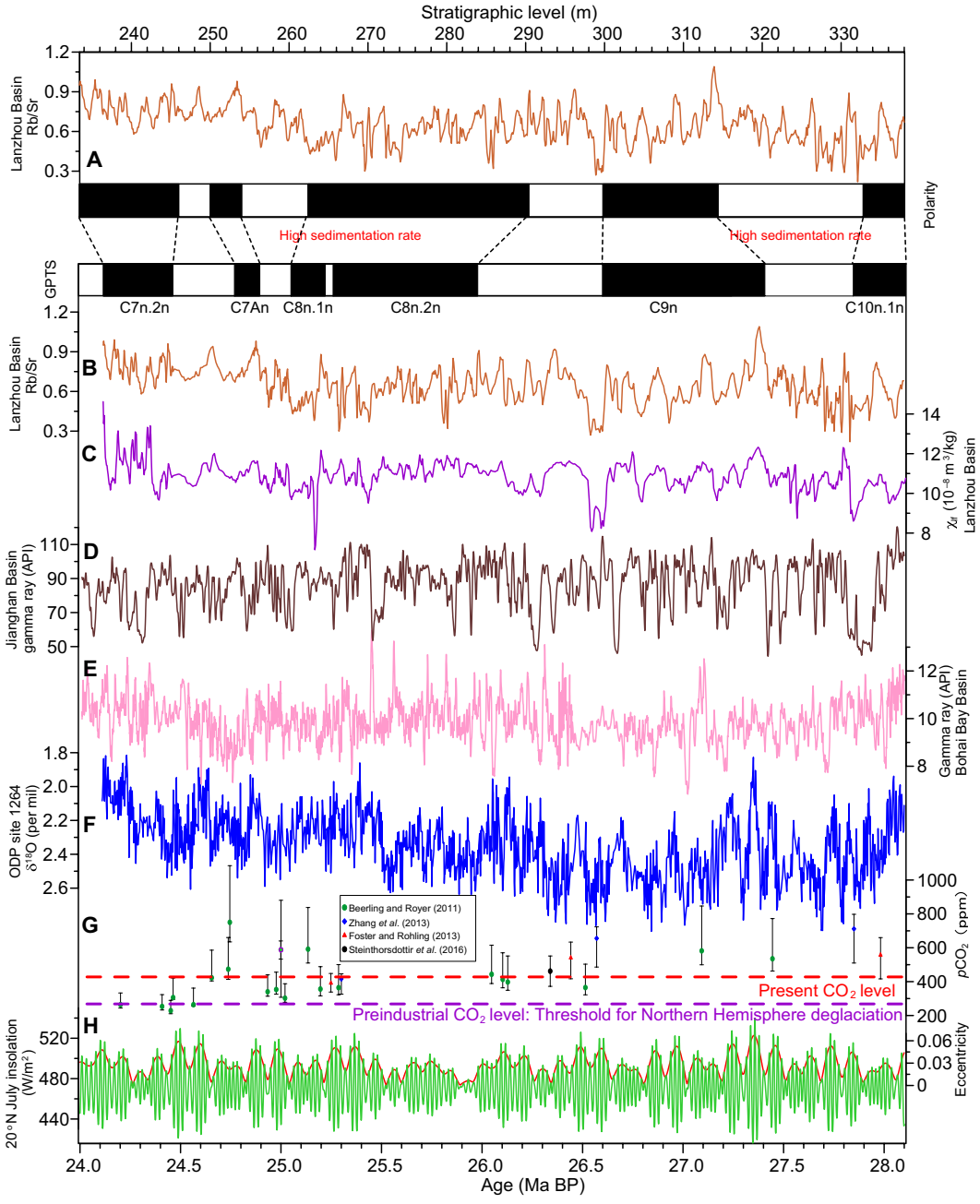

Fig. 2. Global and terrestrial climate changes during the Late Oligocene. (**A**) Paleomagnetic sequence (*15*) and Rb/Sr record of the Duitinggou section plotted versus stratigraphic level. (**B**) Rb/Sr and (**C**) χ_{lf} records plotted on the Duitinggou magnetochronology (*15*) according to the most recent Oligocene geomagnetic polarity time scale (GPTS) (*1*). (**D**) Jianghan Basin gamma ray record (*27*). (**E**) Bohai Bay Basin gamma ray record (*8*). (**F**) ODP Site 1264 benthic foraminiferal $\delta^{18}O$ record (*33*). (**G**) Atmospheric pCO_2 reconstructions (*5*–*8*). (**H**) 20°N July insolation (green curve) and eccentricity (red curve) variability (*34*).

Orbital Asian summer monsoon variability during the Late Oligocene

Pollen analysis of samples taken from our studied section suggests that the Lanzhou Basin had a monsoonal climate during the Late Oligocene, similar to today's subtropical moist climate prevailing in Southeast China (*16*). These paleoclimatic conditions were marked by >800 mm mean annual precipitation, >140 mm mean precipitation in the warmest month, >4 mm precipitation in the coldest month, >10°C mean annual temperature, >23°C mean temperature in the warmest month, and >0°C mean temperature in the coldest month (*16*). Temporal and spatial distributions of carbonate $\delta^{18}O$ and $\delta^{13}C$ across Asia support the notion that, during the Oligocene, regional moisture in the Lanzhou Basin was predominantly transported by the Asian summer monsoon from the western Pacific and Northern Indian Oceans, with a smaller additional winter moisture transport by the westerlies from the shallow proto-Paratethys Sea (*25*),

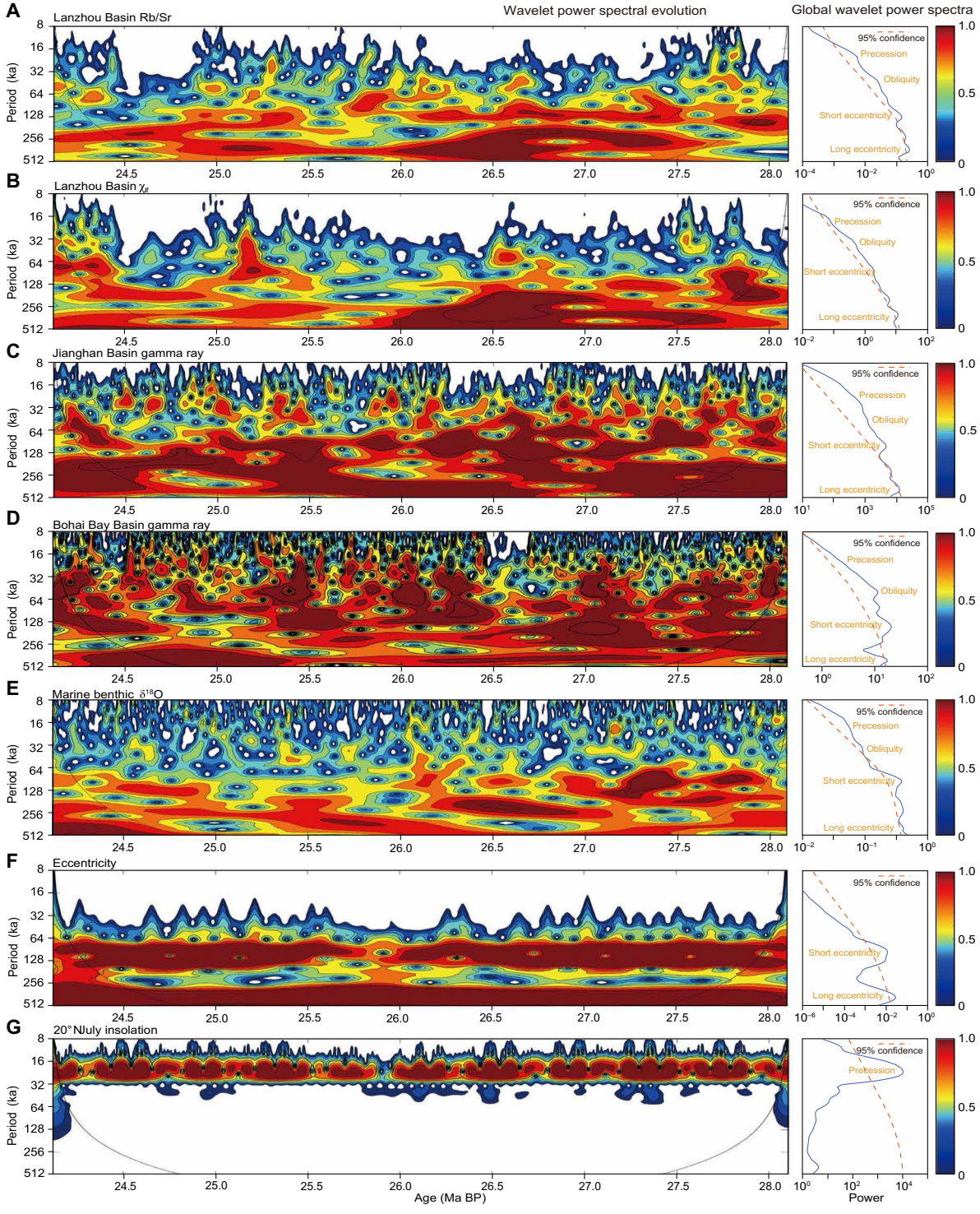

Fig. 3. Orbital climate variability during the Late Oligocene. Wavelet power spectral evolution and global wavelet power spectra for (**A**) Rb/Sr and (**B**) χ_{lf} of the Duitinggou section (Lanzhou Basin) in the untuned magnetochronology (*15*), (**C**) Jianghan Basin gamma ray record (*27*), (**D**) Bohai Bay Basin gamma ray record (*8*), (**E**) ODP Site 1264 benthic foraminiferal $\delta^{18}O$ record (*33*), (**F**) eccentricity (*34*), and (**G**) 20°N July insolation (*34*).

which was located to the west of the Tibetan Plateau (Fig. 1A) (*26*). Thus, the high-resolution Rb/Sr and χ_{lf} records from the Lanzhou Basin, which reflect regional pedogenesis and magnetic mineral transport, were predominantly controlled by changes in summer monsoon precipitation on orbital time scales. We realize, however, that additional secondary influences of temperature, winter precipitation, and seasonality cannot be fully excluded. These records offer an important opportunity to explore the dynamics of

orbital-scale Asian summer monsoon variability during the early stage of a newly established unipolar icehouse state that followed the initial Antarctic glaciation across the EOT. Consistent with the Lanzhou Basin records, the summer monsoon proxy records from Late Oligocene lacustrine sequences in the Jianghan and Bohai Bay Basins, East China (*27*, *28*), also show distinct short and long eccentricity cycles, with a weaker expression of obliquity and precession (Figs. 2, D and E, and 3, C and D). The consistent expression of prominent eccentricity cycles in the various Late Oligocene monsoon proxy records suggests that the eccentricity variability was a widespread phenomenon of Asian monsoon during the warmer-than-present unipolar icehouse period. In addition, prominent short and long eccentricity cycles are also recognized in hydrological records from the Miocene fluviolacustrine sequence in the Qaidam Basin, NE Tibetan Plateau (*29*), the Late Miocene–Pliocene fluviolacustrine sequence in the Weihe Basin, Central China (*30*), the Late Oligocene lacustrine sequence in the Ebro Basin, NE Spain (*31*), and the Late Oligocene–Early Miocene marine sequence from Ceará Rise, Atlantic Ocean (*32*). Thus, eccentricity-paced hydroclimate changes were possibly a widespread, perhaps global, phenomenon during both the Oligocene and Neogene unipolar icehouse states.

Paleoclimatic interpretations based on, among other datasets, a marine benthic foraminiferal $\delta^{18}O$ record from Ocean Drilling Program (ODP) Site 1264 suggest that a large continental-scale ice sheet already existed on Antarctica throughout the Late Oligocene (*33*). Detailed astrochronology together with wavelet analysis indicate that this ice sheet responded in phase lock with eccentricity (Figs. 2, F and H, and 3, E to G) (*33*). The influence of eccentricity on summer insolation is too feeble to force the climate-cryosphere system directly (Fig. 2H) (*34*), thereby invoking the need for a nonlinear response mechanism to eccentricity modulation of precession, the largest contributor to mid- to low-latitude summer insolation variability (Figs. 2H and 3, F and G) (*33*). Like the Lanzhou Basin Rb/Sr and χ_{lf} records, the ODP Site 1264 benthic $\delta^{18}O$ record has a much weaker obliquity expression compared to the short and long eccentricity cycles (Fig. 3E). The precession periodicity is only observed in a few, relatively short-lasting intervals (Fig. 3E). The broadly consistent prevalence of prominent eccentricity cycles in both monsoon and deep-ocean temperature/Antarctic cryosphere proxy records suggests teleconnections among astronomical forcing (i.e., insolation), the mid- to low-latitude monsoon dynamics over Asian continent, and the waxing and waning of the Antarctic Ice Sheet in the warmer-than-present unipolar icehouse world of the Late Oligocene. Potentially, these climate-cryosphere systems were amplified by atmospheric CO_2 concentrations fluctuating between ~400 and ~800 ppm (Fig. 2G) (*5*–*8*).

Three interconnected processes related to Antarctic Ice Sheet fluctuations could have affected moisture transport to the Lanzhou Basin on eccentricity time scales during the Oligocene. First, eccentricity-paced glacial-interglacial Antarctic Ice Sheet fluctuations were generally associated with large-amplitude global temperature changes on eccentricity time scales, which, in turn, would have had a profound influence on the Asian monsoon moisture transport. In this scenario, lower temperatures during Antarctic glacial periods, which are concurrent with eccentricity minima, would have reduced the capacity of the Asian monsoon to transport moisture due to weakening of summer monsoon circulation and decreased moisture availability due to reduction in latent heat flux, moisture evaporation, and lower-tropospheric water vapor loading in the western Pacific and Indian Oceans. Second, lower temperatures during glacial intervals would have displaced the intertropical convergence zone (ITCZ) and summer monsoon southward and the Pacific Walker Cell eastward (*12*), again leading to lower precipitation in the Lanzhou basin. Third, sea level fluctuations during the Late Oligocene Antarctic glacial-interglacial cycles could have driven changes in the monsoonal moisture transport pathway from the western Pacific Ocean to the Lanzhou Basin, leading yet again to variable monsoon precipitation. Higher (lower) sea level resulted in shorter (longer) monsoon moisture transport pathways and higher (lower) precipitation in the Lanzhou Basin (*12*). However, Late Oligocene Antarctic glacial-interglacial cycles resulted in approximately 40-m sea level fluctuations (*35*), which may have been too small to exert a major influence on the precipitation over the Lanzhou Basin. Global temperature fluctuations, driven by glacial-interglacial Antarctic Ice Sheet changes, may have a more profound influence on monsoon precipitation than ice sheet–induced sea level fluctuations.

In addition to the Antarctic Ice Sheet forcing, the prominent eccentricity variability of Asian summer monsoon could also stem directly from eccentricity modulation of low-latitude summer insolation through a nonlinear interaction with the carbon cycle (*36*). Wavelet analysis of the eccentricity solution depicts the variable amplitude and near-continuous presence of the ~110- and 405-ka cycles throughout the Late Oligocene, broadly consistent with the observed major orbital periodicities in the Asian summer monsoon records (Fig. 3). In contrast to obliquity that predominantly influences temperatures at high latitudes, eccentricity modulates summer insolation through its effect on precession (Fig. 2H), which affects temperature and seasonality at mid- to low latitudes (*37*). While low-latitude summer insolation is dominated by precession cycles, direct forcing by short and long eccentricity cycles is negligible (Figs. 2H and 3, F and G). Therefore, it is possible that eccentricity modulation of precession-dominated low-latitude summer insolation caused the Asian monsoon response on eccentricity time scales through nonlinear interactions with the global carbon cycle (*36*). This may have led to a transfer of the eccentricity signal into the Asian monsoon system, with distinct coexisting short and long eccentricity cycles as expressed in our Late Oligocene monsoon records from the Lanzhou Basin. Many orbital forcing hypotheses suggest such a low-latitude origin for eccentricity signals in global climate records, including those based on Cenozoic benthic foraminiferal $\delta^{18}O$ records (*33*, *38*, *39*). By invoking a nonlinear response of the global carbon cycle to precession-dominated insolation forcing at the lower latitudes, we can explain the eccentricity pacing of monsoon variability. Because of the long residence time of carbon in the ocean, the eccentricity periodicities are amplified (*36*).

At first glance, the prominent short eccentricity cyclicity of the summer monsoon during the Late Oligocene is quite similar to observations from Quaternary Chinese Loess Plateau and Nihewan Basin (North China) monsoon records spanning the last ~1 Ma (*40*, *41*). However, younger Quaternary scenarios are suggested to stem predominantly from mid- to high-latitude atmospheric processes forced by the nearby (relative to Antarctic Ice Sheet) Northern Hemisphere ice sheet forcing (*40*, *41*), which contrast with mid- to low-latitude processes induced by low-latitude "eccentricity forcing" and their resonance with the remote Antarctic Ice Sheet during the much warmer Oligocene epoch. In addition, the same oceanic and atmospheric circulation patterns responsible for the Asian summer monsoon intensity and displacements may have also

redirected the poleward atmospheric heat and moisture transport and westerlies in the Southern Hemisphere during the Late Oligocene, which is crucial for Antarctic Ice Sheet growth. It is thus possible that orbitally paced monsoon variability also facilitated glacial-interglacial cycles of the early Antarctic Ice Sheet.

Our sampling resolution of ~4 ka is above the Nyquist frequency of obliquity (*42*), but both Rb/Sr and χ_{lf} records only contain weak obliquity signals (Fig. 3, A and B). Monsoon records from the Jianghan and Bohai Bay Basins (East China) have a similar weak obliquity expression, although the Bohai Bay Basin record, which is from higher

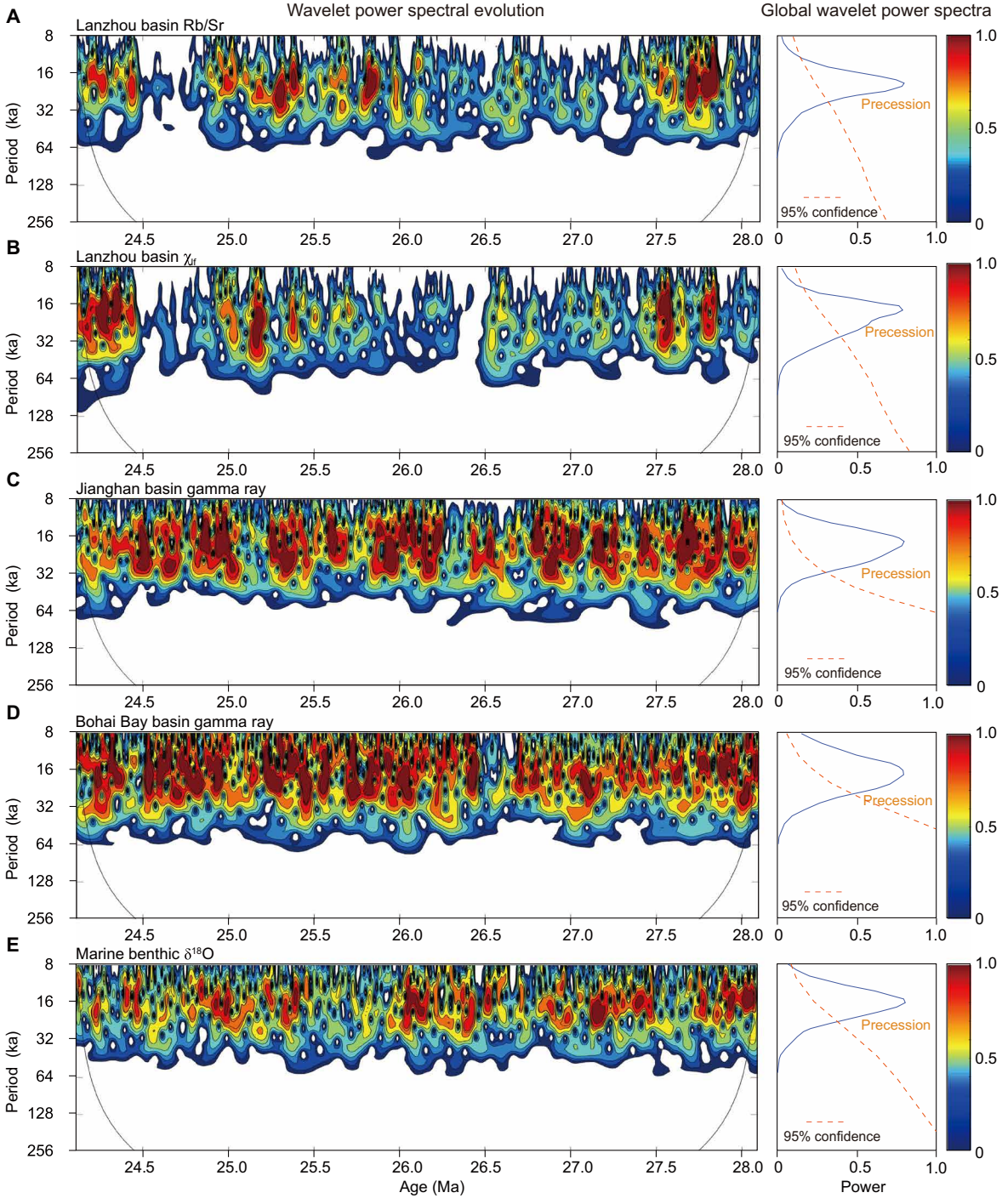

Fig. 4. Precession variability in the Asian monsoon and global climate during the Oligocene. Wavelet power spectral evolution and global wavelet power spectrum for (**A**) Rb/Sr and (**B**) χ_{lf} of the Duitinggou section (Lanzhou Basin), (**C**) Jianghan Basin gamma ray record (*27*), (**D**) Bohai Bay Basin gamma ray record (*8*), and (**E**) ODP Site 1264 benthic foraminiferal $\delta^{18}O$ record (*33*) after removal of longer (>40-ka) periodicities (obliquity and eccentricity) from the data with local regression smoothing to assess a potential precession signal. Note that this wavelet analysis is conducted on the same age model as before the removal (Fig. 3). Before removal, the precession signal is overprinted by stronger eccentricity and obliquity. After removal, a distinct precession signal appears.

latitudes and closer to the western Pacific Ocean, has a stronger obliquity signal than the records from the Lanzhou and Jianghan Basins (Fig. 3) (*27*, *28*). A weaker expression of obliquity than eccentricity might be related to insufficiently large polar ice sheets during the warmer Late Oligocene. The absence of a well-established Northern Hemisphere ice sheet and insufficient extension of Antarctic Ice Sheet into marine environments would have muted climate response to the obliquity forcing (*1*, *43*).

Despite prominent eccentricity cycles, the precession expression is weak in the Rb/Sr and χ_{lf} records from the Lanzhou Basin, gamma ray data from the Jianghan (*27*) and Bohai Bay Basins (*8*), and in ODP Site 1264 benthic $\delta^{18}O$ data (*33*). This may be explained in several ways. First, larger-amplitude and longer periodicities, particularly the prominent short and long eccentricity periodicities, tend to overprint the smaller-amplitude precession signal. Support of this inference is the clear precession expression in spectral analyses of the Late Oligocene Rb/Sr and χ_{lf} data from the Lanzhou Basin, gamma ray data from the Jianghan (*27*) and Bohai Bay Basins (*8*), and ODP Site 1264 benthic $\delta^{18}O$ data (*33*) after removal of the longer (>40-ka) periodicities (Fig. 4). Furthermore, large age uncertainties in the untuned paleomagnetic age model may attenuate true precession signals in the data. In addition, low sedimentation rates, insufficient sampling resolution, and/or strong smoothing effects related to post-depositional diagenesis and biological disturbance have been shown to affect higher frequency signals (precession) in pre-Quaternary records (*29*, *44*).

To summarise, the ~4-Ma-long high-resolution Lanzhou Basin precipitation proxy records provide a unique perspective on orbital-scale Asian monsoon variability on the NE Tibetan Plateau during the Late Oligocene (28.1 to 24.1 Ma BP). This Late Oligocene world was marked by a well-developed monsoonal system that operated under high CO_2 and warm conditions, similar to climate model projections of the near future. The records show dominant short and long eccentricity periodicities with weaker obliquity and precession periodicities, which are broadly in pace with eccentricity and Antarctic Ice Sheet fluctuations. We argue that, in the absence of large Northern Hemisphere ice sheets, changes in atmospheric and oceanic circulation patterns drove Asian summer monsoon variability on orbital time scales. These orbital-scale changes were induced by eccentricity-modulated variations in low-latitude summer insolation and occurred in unison with Antarctic Ice Sheet oscillations. Our comprehensive analyses suggest that the prevalent eccentricity pacing of the Late Oligocene Antarctic Ice Sheet was not an isolated cryospheric phenomenon, but that it was coupled to low-latitude climate systems that also fluctuated over eccentricity cycles, probably through interaction with the global carbon cycle. This finding offers a global perspective on interactions between mid- to low-latitude monsoon systems and high-latitude Antarctic ice volume oscillations. The prevalence of prominent eccentricity cyclicity in both Asian monsoon and Antarctic ice volume during the Late Oligocene, a time of elevated atmospheric CO_2 concentrations relative to preindustrial values, highlights that this orbital response may be more ubiquitous in various paleoclimate systems than previously thought, particularly during warmer periods when the Northern Hemisphere was ice free. These results may be also helpful to future studies that aim to better understand the underlying mechanisms for the mid-Pleistocene transition that marks a major transition of glacial cycles from predominantly lower-amplitude obliquity to larger-amplitude short eccentricity cycles between ~1.25 and 0.6 Ma BP. During this much younger Quaternary period, permanent ice sheets were present in the Northern Hemisphere, but the interplay between low-latitude monsoon systems and high-latitude ice sheets over orbital time scales remains enigmatic.

MATERIALS AND METHODS

After removal of the weathered outcrop surface (at least the topmost 30 cm), we collected 937 samples at ~10-cm intervals for Rb/Sr and χ_{lf} measurements in the laboratory at the Institute of Earth Environment, Chinese Academy of Sciences, Xi'an, China. About 5 g of each sample was ground to <38 μm (passing a 200-mesh sieve) with an agate mortar and pestle. Powders were then used to determine Rb and Sr concentrations with an Innov-X Systems X-ray fluorescence spectrometer in soil mode using a tantalum X-ray tube operated at 50 kV in beam I, 40 kV in beam II, and 15 kV in beam III. The measurement time for each sample was at least 60 s. About 10 g of each sample was powdered and were then packed into nonmagnetic cubic boxes (2 cm × 2 cm × 2 cm) for low-field magnetic susceptibility (χ_{lf}) measurement with a Bartington Instruments MS2 magnetic susceptibility meter at 470 Hz.

Rb/Sr and χ_{lf} records from the Lanzhou Basin, gamma ray records from the Jianghan (*27*) and Bohai Bay Basins (*8*), and ODP Site 1264 benthic foraminiferal $\delta^{18}O$ record (*33*) were all subjected to spectral analysis to evaluate the robustness of their potential orbital signature. First, to obtain evenly spaced data series for spectral analyses, we used the interpolating function in the Acycle software (*45*) to conservatively resample the Rb/Sr and χ_{lf} records at a 3-ka interval, the Jianghan and Bohai Bay Basins gamma ray record at a 1-ka interval, and the ODP Site 1264 benthic $\delta^{18}O$ record at a 2-ka interval. These resampled data series, without detrending, were subsequently used to calculate the wavelet power spectral evolution and global wavelet power spectra using the Acycle software (*45*). The wavelet power spectral evolution was calculated with the following parameters: one-dimensional continuous wavelet transformation with optional significance testing, Morlet wavelet ($k0 = 6$), test periods ranging from 2 to 1000 ka with a discrete scale spacing of 0.1, and cone of influence [as defined by Torrence and Compo (*46*)] = 2^(1/2) × scale. The global wavelet power spectra were calculated with the fast Fourier transform (*46*), with the 95% significance level being calculated using the 2π multi-taper method with the classic first-order autoregressive AR(1) model (*47*).

SUPPLEMENTARY MATERIALS

Supplementary material for this article is available at https://science.org/doi/10.1126/sciadv.abk2318

REFERENCES AND NOTES

1. T. Westerhold, N. Marwan, A. J. Drury, D. Liebrand, C. Agnini, E. Anagnostou, J. S. K. Barnet, S. M. Bohaty, D. De Vleeschouwer, F. Florindo, T. Frederichs, D. A. Hodell, A. E. Holbourn, D. Kroon, V. Lauretano, K. Littler, L. J. Lourens, M. Lyle, H. Pälike, U. Röhl, J. Tian, R. H. Wilken, P. A. Wilson, J. C. Zachos, An astronomically dated record of Earth's climate and its predictability over the last 66 million years. *Science* **369**, 1383–1387 (2020).
2. M. E. Raymo, The initiation of Northern Hemisphere glaciation. *Annu. Rev. Earth Planet. Sci.* **22**, 353–383 (1994).
3. G. H. Haug, A. Ganopolski, D. M. Sigman, A. Rosell-Mele, G. E. A. Swann, R. Tiedemann, S. L. Jaccard, J. Bollmann, M. A. Maslin, M. J. Leng, G. Eglinton, North Pacific seasonality and the glaciation of North America 2.7 million years ago. *Nature* **433**, 821–825 (2005).
4. C. L. O'Brien, M. Huber, E. Thomas, M. Pagani, J. M. Super, L. E. Elder, P. M. Hull, The enigma of Oligocene climate and global surface temperature evolution. *Proc. Natl. Acad. Sci. U.S.A.* **117**, 25302–25309 (2020).

5. G. L. Foster, E. J. Rohling, Relationship between sea level and climate forcing by CO_2 on geological timescales. *Proc. Natl. Acad. Sci. U.S.A.* **110**, 1209–1214 (2013).
6. D. J. Beerling, D. L. Royer, Convergent cenozoic CO_2 history. *Nat. Geosci.* **4**, 418–420 (2011).
7. Y. G. Zhang, M. Pagani, Z. H. Liu, S. M. Bohaty, R. DeConto, A 40-million-year history of atmospheric CO_2. *Phil. Trans. R. Soc. A.* **371**, 20130096 (2013).
8. M. Steinthorsdottir, A. S. Porter, A. Holohan, L. Kunzmann, M. Collinson, J. C. McElwain, Fossil plant stomata indicate decreasing atmospheric CO_2 prior to the Eocene-Oligocene boundary. *Clim. Past* **12**, 439–454 (2016).
9. J. E. Tierney, C. J. Poulsen, I. P. Montañez, T. Bhattacharya, R. Feng, H. L. Ford, B. Hönisch, G. N. Inglis, S. V. Petersen, N. Sagoo, C. R. Tabor, K. Thirumalai, J. Zhu, N. J. Burls, G. L. Foster, Y. Goddéris, B. T. Huber, L. C. Ivany, S. K. Turner, D. J. Lunt, J. C. McElwain, B. J. W. Mills, B. L. Otto-Bliesner, A. Ridgwell, Y. G. Zhang, Past climates inform our future. *Science* **370**, eaay3701 (2020).
10. R. M. DeConto, D. Pollard, P. A. Wilson, H. Pälike, C. H. Lear, M. Pagani, Thresholds for Cenozoic bipolar glaciation. *Nature* **455**, 652–656 (2008).
11. P. X. Wang, Global monsoon in a geological perspective. *Chin. Sci. Bull.* **54**, 1113–1136 (2009).
12. J. W. Beck, W. Zhou, C. Li, Z. K. Wu, L. White, F. Xian, X. H. Kong, Z. S. An, A 550,000-year record of East Asian monsoon rainfall from ^{10}Be in loess. *Science* **360**, 877–881 (2018).
13. Z. S. An, G. X. Wu, J. P. Li, Y. B. Sun, Y. M. Liu, W. J. Zhou, Y. J. Cai, A. M. Duan, L. Li, J. Y. Mao, H. Cheng, Z. G. Shi, L. C. Tan, H. Yan, H. Ao, H. Chang, J. Feng, Global monsoon dynamics and climate change. *Annu. Rev. Earth Planet. Sci.* **43**, 29–77 (2015).
14. A. Farnsworth, D. J. Lunt, S. A. Robinson, P. J. Valdes, W. H. G. Roberts, P. D. Clift, P. Markwick, T. Su, N. Wrobel, F. Bragg, S.-J. Kelland, R. D. Pancost, Past East Asian monsoon evolution controlled by paleogeography, not CO_2. *Sci. Adv.* **5**, aax1697 (2019).
15. P. Zhang, H. Ao, M. J. Dekkers, Z. S. An, L. J. Wang, Y. X. Li, S. H. Liu, X. K. Qiang, H. Chang, H. Zhao, Magnetochronology of the Oligocene mammalian faunas in the Lanzhou Basin, Northwest China. *J. Asian Earth Sci.* **159**, 24–33 (2018).
16. Y. F. Miao, F. L. Wu, M. Herrmann, X. L. Yan, Q. Q. Meng, Late early Oligocene East Asian summer monsoon in the NE Tibetan Plateau: Evidence from a palynological record from the Lanzhou Basin, China. *J. Asian Earth Sci.* **75**, 46–57 (2013).
17. W. T. Wang, P. Z. Zhang, C. C. Liu, D. W. Zheng, J. X. Yu, W. J. Zheng, Y. Z. Wang, H. P. Zhang, X. Y. Chen, Pulsed growth of the West Qinling at ~30Ma in northeastern Tibet: Evidence from Lanzhou Basin magnetostratigraphy and provenance. *J. Geophys. Res.* **121**, 7754–7774 (2016).
18. Z. X. Qiu, B. Y. Wang, Z. D. Qiu, G. P. Xie, J. Y. Xie, X. M. Wang, in *Evidence for Evolution, Essays in Honor of Prof. Chungchien Young on the Hundredth Anniversary of His Birth*, Y. S. Tong, Y. Y. Zhang, W. Y. Wu, J. L. Li, L. Q. Shi, Eds. (China Ocean Press, 1997), pp. 177–192.
19. X. M. Wang, W. Downs, J. Y. Xie, G. P. Xie, *Didymoconus* (mammalia: Didymoconidae) from Lanzhou Basin, China and its stratigraphic and ecological significance. *J. Vertebr. Paleontol.* **21**, 555–564 (2001).
20. Z. X. Wang, Z. Zhang, C. J. Huang, J. M. Shen, Y. Sui, Z. Q. Qiang, Astronomical forcing of lake evolution in the Lanzhou Basin during early Miocene period. *Earth Planet. Sci. Lett.* **554**, 116648 (2021).
21. H. Ao, G. Dupont-Nivet, E. J. Rohling, P. Zhang, J.-B. Ladant, A. P. Roberts, A. Licht, Q. S. Liu, Z. H. Liu, M. J. Dekkers, H. K. Coxall, Z. D. Jin, C. J. Huang, G. Q. Xiao, C. J. Poulsen, N. Barbolini, N. Meijer, Q. Sun, X. K. Qiang, J. Yao, Z. S. An, Orbital climate variability on the northeastern Tibetan Plateau across the Eocene–Oligocene transition. *Nat. Commun.* **11**, 5249 (2020).
22. F. H. Chen, J. H. Chen, J. Holmes, I. Boomer, P. Austin, J. B. Gates, N. L. Wang, S. J. Brooks, J. W. Zhang, Moisture changes over the last millennium in arid central Asia: A review, synthesis and comparison with monsoon region. *Quat. Sci. Rev.* **29**, 1055–1068 (2010).
23. A. Licht, M. van Cappelle, H. A. Abels, J.-B. Ladant, J. Trabucho-Alexandre, C. France-Lanord, Y. Donnadieu, J. Vandenberghe, T. Rigaudier, C. Lécuyer, D. Terry, R. Adriaens, A. Boura, Z. Guo, A. N. Soe, J. Quade, G. Dupont-Nivet, J.-J. Jaeger, Asian monsoons in a late Eocene greenhouse world. *Nature* **513**, 501–506 (2014).
24. G. Dupont-Nivet, W. Krijgsman, C. G. Langereis, H. A. Abels, S. Dai, X. M. Fang, Tibetan Plateau aridification linked to global cooling at the Eocene–Oligocene transition. *Nature* **445**, 635–638 (2007).
25. J. K. C. Rugenstein, C. P. Chamberlain, The evolution of hydroclimate in Asia over the Cenozoic: A stable-isotope perspective. *Earth Sci. Rev.* **185**, 1129–1156 (2018).
26. F. Poblete, G. Dupont-Nivet, A. Licht, D. J. J. Van Hinsbergen, P. Roperch, M. G. Mihalynuk, S. T. Johnston, F. Guillocheau, G. Baby, F. Fluteau, C. Robin, T. J. M. Van Der Linden, D. Ruiz, M. L. J. Baatsen, Towards interactive global paleogeographic maps, new reconstructions at 60, 40 and 20 Ma. *Earth Sci. Rev.* **214**, 103508 (2021).
27. C. J. Huang, L. Hinnov, Astronomically forced climate evolution in a saline lake record of the middle Eocene to Oligocene, Jianghan Basin, China. *Earth Planet. Sci. Lett.* **528**, 115846 (2019).
28. W. Du, Y. L. Ji, G. Chen, H. Wu, C. L. Gao, S. M. Li, Y. Zhang, Cyclostratigraphy and astronomical tuning during the Oligocene in the Jizhong Depression, Bohai Bay Basin, northeastern China. *Palaeogeogr. Palaeoclimatol. Palaeoecol.* **554**, 109803 (2020).
29. J. S. Nie, C. Garzione, Q. D. Su, Q. S. Liu, R. Zhang, D. Heslop, C. Necula, S. H. Zhang, Y. G. Song, Z. Luo, Dominant 100,000-year precipitation cyclicity in a late Miocene lake from northeast Tibet. *Sci. Adv.* **3**, 1600762 (2017).
30. Y. C. Wang, H. Y. Lu, K. X. Wang, Y. Wang, Y. X. Li, S. Clemens, H. Z. Lv, Z. H. Huang, H. L. Wang, X. Z. Hu, F. Z. Lu, H. Z. Zhang, Combined high- and low-latitude forcing of East Asian monsoon precipitation variability in the Pliocene warm period. *Sci. Adv.* **6**, eabc2414 (2020).
31. L. Valero, M. Garcés, L. Cabrera, E. Costa, A. Sáez, 20 Myr of eccentricity paced lacustrine cycles in the Cenozoic Ebro Basin. *Earth Planet. Sci. Lett.* **408**, 183–193 (2014).
32. N. J. Shackleton, S. J. Crowhurst, G. P. Weedon, J. Laskar, Astronomical calibration of Oligocene–Miocene time. *Philos. Trans. R. Soc., Math. Phys. Eng. Sci.* **357**, 1907–1929 (1999).
33. D. Liebrand, A. T. M. de Bakker, H. M. Beddow, P. A. Wilson, S. M. Bohaty, G. Ruessink, H. Pälike, S. J. Batenburg, F. J. Hilgen, D. A. Hodell, C. E. Huck, D. Kroon, I. Raffi, M. J. M. Saes, A. E. van Dijk, L. J. Lourens, Evolution of the early Antarctic ice ages. *Proc. Natl. Acad. Sci. U.S.A.* **114**, 3867–3872 (2017).
34. J. Laskar, A. Fienga, M. Gastineau, H. Manche, La2010: A new orbital solution for the long-term motion of the Earth. *Astron. Astrophys.* **532**, A89 (2011).
35. T. R. Naish, G. S. Wilson, G. B. Dunbar, P. J. Barrett, Constraining the amplitude of Late Oligocene bathymetric changes in western Ross Sea during orbitally-induced oscillations in the East Antarctic Ice Sheet: (2) Implications for global sea-level changes. *Palaeogeogr. Paleoclimatol. Palaeocl.* **260**, 66–76 (2008).
36. H. Pälike, R. D. Norris, J. O. Herrle, P. A. Wilson, H. K. Coxall, C. H. Lear, N. J. Shackleton, A. K. Tripati, B. S. Wade, The heartbeat of the Oligocene climate system. *Science* **314**, 1894–1898 (2006).
37. T. Laepple, G. Lohmann, Seasonal cycle as template for climate variability on astronomical timescales. *Paleoceanography* **24**, PA4201 (2009).
38. S. C. Clemens, R. Tiedemann, Eccentricity forcing of Pliocene early Pleistocene climate revealed in a marine oxygen-isotope record. *Nature* **385**, 801–804 (1997).
39. D. Liebrand, A. T. M. de Bakker, Bispectra of climate cycles show how ice ages are fuelled. *Clim. Past* **15**, 1959–1983 (2019).
40. X. Z. Peng, H. Ao, G. Q. Xiao, X. K. Qiang, Q. Sun, The Early–Middle Pleistocene transition of Asian summer monsoon. *Palaeogeogr. Palaeoclimatol. Palaeoecol.* **545**, 109636 (2020).
41. H. Ao, M. J. Dekkers, G. Q. Xiao, X. Q. Yang, L. Qin, X. D. Liu, X. K. Qiang, H. Chang, H. Zhao, Different orbital rhythms in the Asian summer monsoon records from North and South China during the Pleistocene. *Glob. Planet. Change* **80**, 51–60 (2012).
42. D. Liebrand, H. M. Beddow, L. J. Lourens, H. Pälike, I. Raffi, S. M. Bohaty, F. J. Hilgen, M. J. M. Saes, P. A. Wilson, A. E. van Dijk, D. A. Hodell, D. Kroon, C. E. Huck, S. J. Batenburg, Cyclostratigraphy and eccentricity tuning of the early Oligocene through early Miocene (30.1–17.1 Ma): *Cibicides mundulus* stable oxygen and carbon isotope records from Walvis Ridge Site 1264. *Earth Planet. Sci. Lett.* **450**, 392–405 (2016).
43. R. H. Levy, S. R. Meyers, T. R. Naish, R. N. Golledge, R. M. McKay, J. S. Crampton, R. M. DeConto, L. De Santis, F. Florindo, E. G. W. Gasson, D. M. Harwood, B. P. Luyendyk, R. D. Powell, C. Clowes, D. K. Kulhanek, Antarctic ice-sheet sensitivity to obliquity forcing enhanced through ocean connections. *Nat. Geosci.* **12**, 132–137 (2019).
44. Q. D. Su, J. S. Nie, Z. Luo, M. S. Li, R. Heermance, C. Garzione, Detection of strong precession cycles from the late Pliocene sedimentary records of northeastern Tibetan Plateau. *Geochem. Geophys. Geosyst.* **20**, 3901–3912 (2019).
45. M. S. Li, L. Hinnov, L. Kump, Acycle: Time-series analysis software for paleoclimate research and education. *Comput. Geosci.* **127**, 12–22 (2019).
46. C. Torrence, G. P. Compo, A practical guide to wavelet analysis. *Bull. Am. Meteorol. Soc.* **79**, 61–78 (1998).
47. M. E. Mann, J. M. Lees, Robust estimation of background noise and signal detection in climatic time series. *Clim. Change* **33**, 409–445 (1996).

Acknowledgments: We thank professors Z. D. Jin and C. J. Poulsen for helpful discussions on this paper. **Funding:** This study was supported financially by the Chinese Academy of Sciences (CAS) Strategic Priority Research Program (XDB 40000000), the Second Tibetan Plateau Scientific Expedition and Research (STEP) program (2019QZKK0707), and the National Natural Science Foundation of China (42074076). **Author contributions:** H.A. designed the study. H.A., D.L., M.J.D., P.Z., Y.G.S., Q.S.L, T.N.J., X.Z.L., X.X.L., Q.S., X.K.Q., and Z.S.A. contributed to data analysis, interpretation, and discussion. H.A. wrote the manuscript with contributions from all other authors. **Competing interests:** The authors declare that they have no competing interests. **Data and materials availability:** All data needed to evaluate the conclusions in the paper are present in the paper. The proxy data used to support the major finding of this research are attached in the data file and also available in the East Asian Paleoenvironmental Science Database (http://paleodata.ieecas.cn/index.aspx, data DOI: 10.12262/IEECAS.EAPSD2021003).

Submitted 30 June 2021
Accepted 28 October 2021
Published 15 December 2021
10.1126/sciadv.abk2318

ScienceAdvances

Eccentricity-paced monsoon variability on the northeastern Tibetan Plateau in the Late Oligocene high CO world

Hong AoDiederik LiebrandMark J. DekkersPeng ZhangYougui SongQingsong LiuTara N. JonellQiang SunXinzhou LiXinxia LiXiaoke QiangZhisheng An

Sci. Adv., 7 (51), eabk2318. • DOI: 10.1126/sciadv.abk2318

Science Advances (ISSN) is published by the American Association for the Advancement of Science. 1200 New York Avenue NW, Washington, DC 20005. The title *Science Advances* is a registered trademark of AAAS.